

See discussions, stats, and author profiles for this publication at: <https://www.researchgate.net/publication/273420071>

Density functional theory study into H₂O dissociative adsorption on the Fe₅C₂(010) surface

ARTICLE in APPLIED CATALYSIS A GENERAL · NOVEMBER 2013

Impact Factor: 3.94 · DOI: 10.1016/j.apcata.2013.09.017

CITATIONS

7

READS

7

7 AUTHORS, INCLUDING:



Rui Gao

Chinese Academy of Sciences

4 PUBLICATIONS 12 CITATIONS

[SEE PROFILE](#)



Yong-Wang Li

Chinese Academy of Sciences

403 PUBLICATIONS 6,043 CITATIONS

[SEE PROFILE](#)



Jianguo Wang

Northwestern Polytechnical University

209 PUBLICATIONS 3,274 CITATIONS

[SEE PROFILE](#)



Density functional theory study into H₂O dissociative adsorption on the Fe₅C₂(0 1 0) surface



Rui Gao^a, Dong-Bo Cao^a, Shaoli Liu^a, Yong Yang^a, Yong-Wang Li^a,
Jianguo Wang^a, Haijun Jiao^{a,b,*}

^a State Key Laboratory of Coal Conversion, Institute of Coal Chemistry, Chinese Academy of Sciences, Taiyuan 030001, China

^b Leibniz-Institut für Katalyse e.V. an der Universität Rostock, Albert-Einstein-Strasse 29a, 18059 Rostock, Germany

ARTICLE INFO

Article history:

Received 26 July 2013

Received in revised form 5 September 2013

Accepted 10 September 2013

Available online 19 September 2013

Keywords:

DFT

Iron carbide

H₂O dissociation

Surface oxidation

ABSTRACT

Spin-polarized density functional theory calculations (GGA-PBE) have been carried out to study H₂O adsorption and dissociation on the Fe₅C₂(0 1 0) surface. It is found that the iron region on the Fe₅C₂(0 1 0) surface is active for H₂O adsorption and dissociation, while the carbon region is inactive. For H₂O adsorption in the iron region, H₂O prefers the top site of the surface iron atoms, and significant hydrogen bonding interaction has been found at high H₂O coverage on the basis of the computed adsorption energies and the intermolecular O-H distances. In the iron region H₂O dissociation (H₂O → H + OH; OH → H + O) is favored both kinetically and thermodynamically. On one O pre-covered surface, O-assisted H₂O dissociation becomes favorable kinetically (O + H₂O → OH + OH) and further OH dissociation (OH → H + O) becomes difficult thermodynamically. Upon the increase of surface O coverage, H₂O dissociation becomes difficult, while H₂ formation from the surface adsorbed H atoms becomes easy. On the potential energy surface, the dissociation of four H₂O molecules into four surface O and four H₂ molecules (4H₂O(g) → 4O(s) + 4H₂(g)) is still thermodynamically favorable by 0.63 eV, and the iron region is fully covered by surface oxygen atoms. Thermodynamic analysis reveals clearly that the catalyst surface has always adsorbed oxygen atoms under water environment and their number in the iron region depends on temperature and water content; and high temperature and low H₂O partial pressure can maintain the catalyst stability and excess H₂O partial pressure will result in full oxidation. For the oxidation of one surface carbon atom, it is necessary to migrate one of the four adsorbed oxygen atoms from the iron region to the carbon region, and the H₂O assisted CO₂ formation is more favorable than the direct CO₂ formation. The overall surface carbon oxidation, Fe_xC_y + 4H₂O(g) → O₂Fe_xC_{y-1} + CO₂(g) + 4H₂(g), is thermodynamically accessible. Detailed comparisons show that the Fe(1 0 0) and Fe₅C₂(0 1 0) surfaces are very similar in H₂O adsorption and dissociation at low coverage.

© 2013 Elsevier B.V. All rights reserved.

1. Introduction

Fischer-Tropsch synthesis (FTS) is a key technology in converting synthesis gas (H₂/CO) into fuels and chemicals [1]. In iron-based FTS [2] χ -Fe₅C₂ is one of the active phases and has received high theoretical attention [3]. As one of the FTS side products, H₂O in excess can oxidize iron carbide into magnetite (Fe₃O₄), and it is necessary to study the oxidation of the Fe₅C₂ surface by H₂O for a deeper understanding into the deactivation mechanism of FTS active catalysts.

Experimentally there are many studies about the effect of H₂O on iron-based FTS catalysts [4]. H₂O is generally believed to promote the oxidation of active iron carbide and thus has an inhibiting effect on the FTS rate [4a–4i]. Thüne et al. [4i] and Pendyala et al. [4j]

demonstrated that the oxidation of iron-based FTS catalysts under high H₂O pressure is very sensitive to reaction temperature and an irreversible process. Under high H₂O pressure, the active surfaces of iron-based FTS catalysts are covered by considerable amounts of adsorbed oxygen, and iron(II)oxide was detected. According to the kinetic models for iron-based FTS, however, Botes et al. [4k] suggested that H₂O may not have a kinetic effect on the FTS activity; and it can only modify the relative CO/H₂ ratio through changing the activity and selectivity of the water-gas shift (WGS) reaction. Theoretically, there are no detailed studies about H₂O adsorption and dissociation on the Fe_xC_y surfaces, apart from only one by Cao et al. [5]. On the basis of density functional theory (DFT) calculations, Cao et al. found that H₂O formation from 2OH → H₂O + O is energetically more favored than from OH + H → H₂O on the Fe₅C₂(0 0 1) surface.

In this work, on the basis of DFT calculations, we investigated the adsorption of H₂O, OH, O and H as well H₂O dissociation at low and higher coverage on the Fe₅C₂(0 1 0) surface. Furthermore, H₂O

* Corresponding author. Tel.: +49 381 1281 135; fax: +49 381 1281 51135.

E-mail address: haijun.jiao@catalysis.de (H. Jiao).

dissociation on oxygen pre-adsorbed surfaces and the oxidation of the surface carbon by the adsorbed O atoms in the iron region were studied as well. It is noted that this is the first time to study the oxidation of iron carbide surface by H₂O, which is helpful to understand the effect of H₂O in FTS.

2. Methods and models

2.1. Methods

All calculations were performed using the plane wave based periodic DFT method as implemented in the Vienna *Ab Initio* Simulation Package (VASP) [6]. The electron-ion interaction was described with the projector augmented wave (PAW) method [7]. The electron exchange and correlation energies were treated within the generalized gradient approximation in the Perdew–Burke–Ernzerhof functional (GGA-PBE) [8]. The plane wave basis was set up to 400 eV, and a $5 \times 3 \times 1$ MP k -point sampling was used. Electron smearing was used via the Methfessel–Paxton technique with a smearing width consistent to $\sigma = 0.2$ eV. Because of the large effect of magnetic properties on the adsorption energies spin polarization was included. All transition states were estimated using the Nudged Elastic Band (NEB) method [9], and we analyzed the stretching frequencies in order to characterize whether a stationary point is a minimum state without imaginary frequency or a transition state with only one imaginary frequency. The frequency calculations provide also zero-point energies (ZPE). For the free adsorbates (X), the ZPE was calculated in gas phase in a $(10 \times 10 \times 10)$ cell. For the bare slab, the vibrational contributions of the first relaxed layer are included. For the slab with adsorbates, we included the vibrational contributions of the first relaxed layer and the adsorbed species.

The adsorption energy was calculated according to $E_{\text{ads}} = E_{\text{X/slab}} - [E_{\text{slab}} + E_{\text{X}}]$, where $E_{\text{X/slab}}$ is the total energy of the slab with adsorbates in its equilibrium geometry, E_{slab} is the total energy of the bare slab, and E_{X} is the total energy of the free adsorbates in the gas phase. Therefore, the more negative the E_{ads} , the stronger the adsorption. The barrier (E_a) and reaction energy (ΔE_r) are calculated according to $E_a = E_{\text{TS}} - E_{\text{IS}}$ and $\Delta E_r = E_{\text{FS}} - E_{\text{IS}}$, where E_{IS} , E_{FS} and E_{TS} are the energies of the corresponding initial state (IS), final state (FS) and transition state (TS), respectively. We present the adsorption energies with ($E_{\text{ads/ZPE}}$) and without (E_{ads}) the ZPE correction. All $E_{\text{ads/ZPE}}$ are used for our discussion, and all E_{ads} are given for comparison. All energetic data (E_a and ΔE_r) on the potential energy surface include the ZPE correction.

2.2. Models

Bulk $\chi\text{-Fe}_5\text{C}_2$ is a monoclinic crystal, and its structure has C2/c crystallographic symmetry and contains 20 Fe and 8 C atoms per unit cell. There are three types of iron atom [with the Wyckoff positions Fe1 (x_1, y_1, z_1) (8f), Fe2 (x_2, y_2, z_2) (8f), Fe3 (0, $y_3, 0.25$) (4e)] and one type of carbon atom [C (x_4, y_4, z_4) (8f)] in the unit cell. The PAW-PBE lattice parameters ($a = 11.545$ Å, $b = 4.496$ Å, $c = 4.982$ Å and $\beta = 97.60^\circ$) have maximal deviation of 1.68% from the experimental values ($a = 11.562$ Å, $b = 4.573$ Å, $c = 5.060$ Å and $\beta = 97.74^\circ$) [10]. Using PAW-PBE we found three different Fe atoms with magnetic moments of 2.125, 1.691 and 1.090 μ_B , and the C atom carries an opposite magnetic moment of $-0.097 \mu_B$. The calculated average magnetic moment on all Fe atoms inside the unit cell is 1.74 μ_B , which is very close to the experimental values (1.72–1.75 μ_B). Therefore, PAW-PBE can reproduce not only the structural parameters but also the magnetic properties of bulk $\chi\text{-Fe}_5\text{C}_2$ very well. Without spin polarization, the unit cell does not have any magnetic moment, which is different from the experimental finding,

and is also less stable than that with spin polarization by 2.67 eV. Therefore, it is necessary to include spin polarization in our calculations.

$\chi\text{-Fe}_5\text{C}_2$ has six surface terminations [11] and $\chi\text{-Fe}_5\text{C}_2(0\ 1\ 0)$ is the most stable one [3e,f]. The $\chi\text{-Fe}_5\text{C}_2(0\ 1\ 0)0.25$ surface is very special, since it has both iron and carbon regions on the outmost layer. Theoretical studies about CO dissociation [3g] and CH₄ formation [12] on this surface are reported. In this work, aiming to provide some information of the iron carbide oxidation, $\chi\text{-Fe}_5\text{C}_2(0\ 1\ 0)$ is also used as surface model to study the mechanism of H₂O dissociation, which is beneficial to understand the FTS along with other reactions. The $\chi\text{-Fe}_5\text{C}_2$ bulk is stoichiometric to the primitive unit cell and has a symmetric termination with top and bottom planes within a periodic layer and each layer has 10 Fe and 4 C atoms (Fig. 1a). In top and side views (Fig. 1b), the configuration of this surface is symmetrical, e.g.; on the surface two prominent C atoms (C₁ and C₂), two hollow C atoms (C₃ and C₄) and four couples of Fe atoms (Fe₁/Fe₂, Fe₃/Fe₄, Fe₅/Fe₆, Fe₇/Fe₈) have identical chemical surroundings, respectively.

In order to choose a reasonable surface model, five slab models with periodic conditions along the $\chi\text{-Fe}_5\text{C}_2(0\ 1\ 0)$ expansion have been used for benchmark testing: (i) two layers of one relaxed and one fixed (1R/1F), (ii) three layers of one relaxed and two fixed (1R/2F), (iii) four layers of one relaxed and three fixed (1R/3F), (iv) four layers of two relaxed and two fixed (2R/2F), and (v) four layers of three relaxed and one fixed (3R/1F). For 1R/1F, 1R/2F and 1R/3F, the computed H₂O adsorption energy (without ZPE correction) is -0.65 , -0.63 and -0.65 eV, respectively. For 2R/2F and 3R/1F, the computed H₂O adsorption energy is -0.65 and -0.65 eV, respectively. In addition, we calculated CO adsorption energy (Supporting information) using the smallest slab model of -2.02 eV agrees perfectly with the reported results of Sorescu using the four-layer model (40 Fe and 16 C) of -2.01 eV for the most stable adsorption site [3f]. Without spin polarization, the computed adsorption energies of CO (-2.25 eV) and H₂O (-0.92 eV) differ from those with spin polarization. It shows clearly that the adsorption energy differences of H₂O and CO between the smallest and the largest models are only 0.01 eV, and we therefore used the smallest 1R/1F model having 20 Fe and 8 C atoms in all calculations.

2.3. Atomistic thermodynamics

To investigate the thermodynamic stability of the surface with adsorbed O atoms under practical condition, we used the atomistic thermodynamic approach [13]. According to the literature description, we can write down the formation process of surface O atoms as the reaction of $\text{Fe}_5\text{C}_2 + n\text{O} \rightarrow n\text{O}/\text{Fe}_5\text{C}_2$, where n denotes the number of O atom adsorbed on the Fe_5C_2 surface. The related reaction Gibbs free energy can be expressed as $\Delta G = G(n\text{O}/\text{Fe}_5\text{C}_2) - G(\text{Fe}_5\text{C}_2) - n\mu(\text{O})$, where $G(n\text{O}/\text{Fe}_5\text{C}_2)$ and $G(\text{Fe}_5\text{C}_2)$ stand for the Gibbs free energies of Fe_5C_2 slab with and without adsorbed O atoms, and $\mu(\text{O})$ stands for the chemical potential of a O atom. Since the vibration terms of the slab does not vary in a very large degree upon O atom adsorption, we neglected their contribution to the Gibbs free energy of the slab with and without adsorbed O atoms, and used only the total energy $E_{n\text{O/slab}}$ and E_{slab} as the predominant terms, which can be calculated directly from DFT, i.e. $G(n\text{O}/\text{Fe}_5\text{C}_2) - G(\text{Fe}_5\text{C}_2) = \Delta G^s \approx \Delta E^s$. For $\mu(\text{O})$, it is expressed as $\mu(\text{O}) = \mu(\text{H}_2\text{O}) - \mu(\text{H}_2)$, then we can simplify the free energy as $\Delta G = \Delta E^s - n[\mu(\text{H}_2\text{O}) - \mu(\text{H}_2)]$. The chemical potentials of gas phase H₂O and H₂ are described in the way of $\mu(p, T) = \mu^\circ(T) + E_{\text{ZPE}} + kT\ln(p/p^\circ)$, in which $\mu^\circ(T)$ and E_{ZPE} stand for chemical potential and the total energy with ZPE correction of H₂O or H₂, respectively. Therefore, the free energy ΔG is equal to $\Delta E^s - n[\Delta\mu^\circ(T) + \Delta E_{\text{ZPE}} + kT\ln(p_{\text{H}_2\text{O}}/p_{\text{H}_2})]$, in which $\Delta\mu^\circ(T) = \mu^\circ(\text{H}_2\text{O}, T) - \mu^\circ(\text{H}_2, T)$ and $\Delta E_{\text{ZPE}} = E_{\text{ZPE}}(\text{H}_2\text{O}) - E_{\text{ZPE}}(\text{H}_2)$.

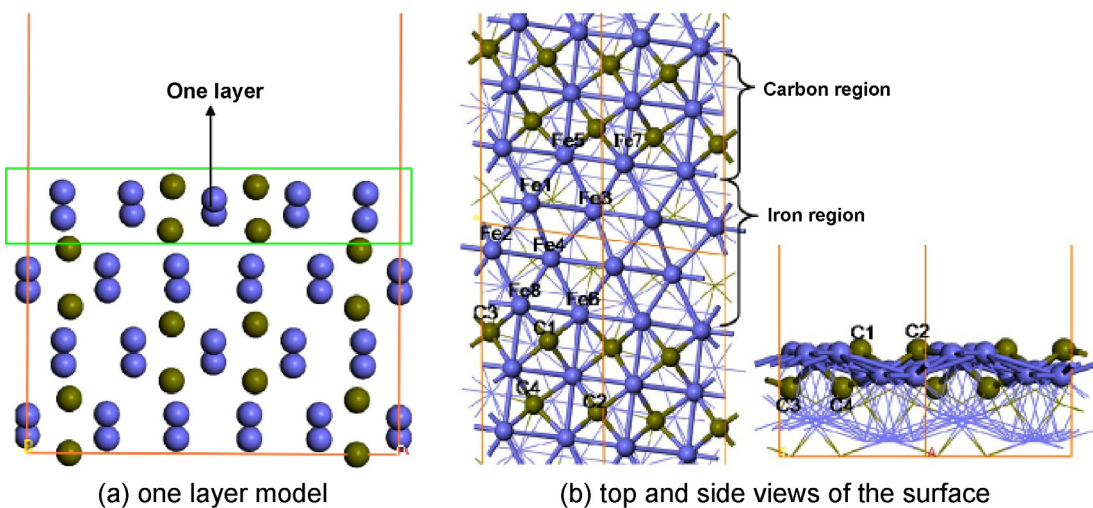


Fig. 1. The χ -Fe₅C₂(0 1 0) surface: (a) the green square represents one periodic layer which consist of 10 Fe and 4 C atoms; (b) top view and side view for the iron and carbon regions (Fe atoms in blue and C atoms in dark orange). (For interpretation of the references to color in this figure legend, the reader is referred to the web version of this article.)

The $\Delta\mu^\circ(T)$ can be found from the thermodynamic data table and the ΔE_{ZPE} can be obtained directly from DFT calculation. The adopted thermodynamic approach estimates only the thermodynamic stability of surface phases at equilibrium state from the reaction; the kinetic parameter needs to be additionally taken into account, and this is beyond the scope of this work.

3. Results and discussion

3.1. Adsorption of H_2O , OH, O and H

The adsorption of H₂O, OH, O and H on the $\chi\text{-Fe}_5\text{C}_2(0\ 1\ 0)$ surface is computed at first. The structures of the most stable adsorption configurations are given in Fig. 2, the computed bond distances and adsorption energies including ZPE corrections are given in Table 1.

In the iron region, H₂O preferably adsorbs on the top site (H₂O_{1F}/-0.51 eV), in agreement with the previous studies [14] and the Fe-OH₂ distance is 2.131 Å. The OH group adsorbs on the bridge site (OH_{2F}/-4.24 eV) with the Fe-OH distance of 1.956 and 1.957 Å. The O and H atoms favorably adsorb on the three-fold hollow sites (O_{3F}/-6.57 eV and H_{3F}/-2.87 eV), and the Fe-O distances are 1.854, 1.906 and 1.914 Å and the Fe-H distances are 1.772, 1.773 and 1.793 Å.

For the co-adsorption of two H₂O molecules, they also prefer the top sites with adsorption energy of -1.18 eV, which is higher than two folds of one H₂O adsorption (-1.02 eV); and the Fe-OH₂ distances are 2.146 and 2.249 Å. This energetic difference can be attributed to the hydrogen bonding between two H₂O molecules; and the intermolecular H...O distance is 1.824 Å. For the co-adsorption of three H₂O molecules, the calculated adsorption energy is -1.79 eV, which is higher than three folds of one H₂O adsorption (-1.53 eV). These indicate again the strong hydrogen bonding interaction from their short intermolecular H...O distances of 1.582 and 1.732 Å. However, the most interesting and important points are their adsorption configurations. For example, there are two short Fe-OH₂ distances (2.134 and 2.150 Å) and one very long Fe-OH₂ distance (3.571 Å), indicating that the third H₂O molecule interacts more strongly with two H₂O molecules instead with the surface Fe atom.

The same phenomena are also found for the co-adsorption of four H₂O molecules. For example, two H₂O molecules have short Fe-OH₂ distances (2.067 and 2.133 Å), and the other two H₂O molecules have very long Fe-OH₂ distances (3.573 and 3.494 Å). In

addition, the co-adsorption energy of -2.33 eV is higher than that of four folds of one H_2O adsorption (-2.04 eV). The intermolecular $\text{H} \dots \text{O}$ distance are 1.615 , 1.680 and 1.828\AA . The stepwise adsorption energy of H_2O of -0.51 , -0.67 , -0.61 and -0.54 eV, shows clearly that the iron region can be covered fully by H_2O molecules.

The computed hydrogen bonding energies are within the range of the reported values (0.1–0.3 eV), and the exact values depend on their geometries and bond lengths [15]. In a mass of works of the adsorption of water clusters on metal surfaces [16], the interaction of H₂O and the metal will be influenced by the hydrogen bonding networks.

In the carbon region, H_2O adsorption on the top site has very low absorption energy ($\text{H}_2\text{O}_{cr-1F}/0.02$ eV, Supporting information). OH adsorbs preferably on the top and bridge sites ($\text{OH}_{cr-1F}/-2.98$ eV and $\text{OH}_{cr-2F}/-2.96$ eV, respectively). The O and H atoms adsorb preferably on the top site ($\text{O}_{cr-1F}/-5.67$ eV and $\text{H}_{cr-1F}/-2.53$ eV, respectively). These indicate the adsorption preference of H_2O , OH, H and O on surface iron region instead of on surface carbon region.

3.2. H_2O direct dissociation ($H_2O = O + H_2(g)$)

On the basis of the most stable adsorption sites of H₂O, OH, O and H, we computed H₂O dissociation in both Fe and C regions. For H₂O dissociation in the Fe region the optimized structures of IS, TS and FS are shown in Fig. 3; the bond lengths of IS and FS are given in Table 1. The barriers, reaction energies and critical bond distances of TS are given in Table 2. The energy profiles are shown in Fig. 4.

On the basis of the most stable H_2O adsorption configuration ($\text{H}_2\text{O}_{1\text{F}}$), H_2O dissociation into $\text{OH} + \text{H}$ is considered. In the transition state (**TS1**), both OH and H locate at top sites of surface iron atoms, and the distance of the forming $\text{Fe}-\text{H}$ and breaking $\text{H}-\text{OH}$ bonds is 1.823 and 1.333 Å, respectively. In the final state ($\text{OH}_{2\text{F}} + \text{H}$), the adsorbed H atom and OH are on the three-fold and the bridge sites, respectively; and the $\text{Fe}-\text{OH}$ distances are 1.965 and 1.943 Å (**Table 1**). The calculated dissociation barrier is 0.47 eV, and the H_2O dissociation energy is exothermic by 1.06 eV.

For OH dissociation, it is necessary to migrate the OH at the bridge site (OH_{2F}) to a metastable three-fold site (OH_{3F}) and this is because that the distance between the H atom in OH_{3F} and the surface iron atom is shorter than that in OH_{2F} ; and the migration barrier is very low (0.15 eV). For $\text{OH} + \text{H}$ dissociation into $\text{O} + 2\text{H}$, starting from $\text{OH}_{3F} + \text{H}$, the barrier is 0.43 eV, and the dissociation step is exothermic by 0.48 eV. In the transition state (**TS2**), the

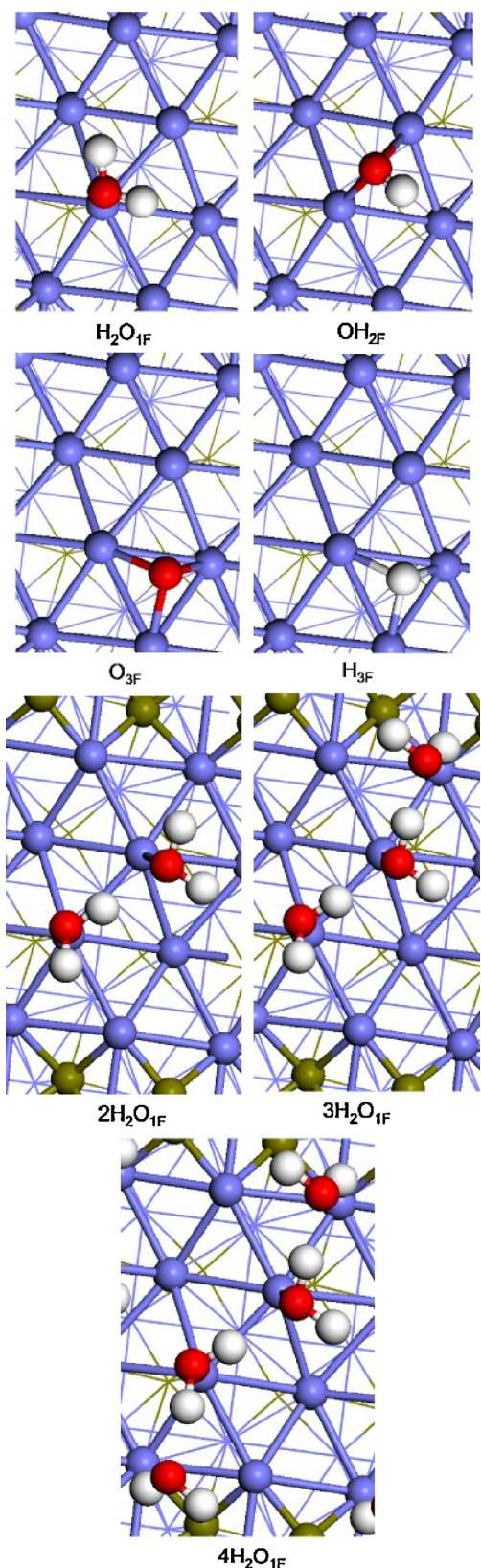


Fig. 2. Most stable adsorption structures for H_2O , OH , O , H , $2\text{H}_2\text{O}$, $3\text{H}_2\text{O}$ and $4\text{H}_2\text{O}$ in the Fe region on the $\text{Fe}_5\text{C}_2(0\ 1\ 0)$ surface (Fe atom in blue, C atom in dark orange, O atom in red and H atom in white). (For interpretation of the references to color in this figure legend, the reader is referred to the web version of this article.)

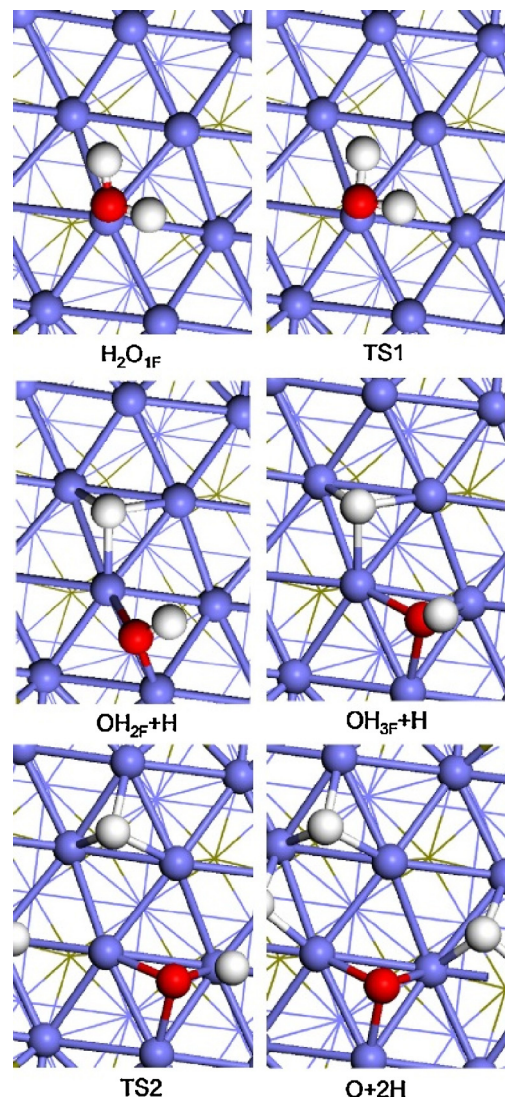


Fig. 3. Key surface structures of one H_2O direct dissociation in the Fe region on the $\text{Fe}_5\text{C}_2(0\ 1\ 0)$ surface (Fe atom in blue, O atom in red and H atom in white). (For interpretation of the references to color in this figure legend, the reader is referred to the web version of this article.)

distance of the forming $\text{Fe}-\text{H}$ and the breaking $\text{O}-\text{H}$ is 1.637 and 1.359 Å, respectively. During the $\text{O}-\text{H}$ dissociation, the previously dissociated H atom moves from one 3-fold site to another 3-fold site. In the final state ($\text{O} + 2\text{H}$), both the O atom and the two H atoms are located at the 3-fold sites.

For the formation of gaseous H_2 from $\text{O} + 2\text{H}$, the transition state could not be located, and this is because that the most stable state of molecular H_2 adsorption on one O pre-covered surface is dissociative, and surface $\text{O} + 2\text{H}$ should be the most stable intermediates. The formation of H_2 from $\text{O} + 2\text{H}$ is endothermic by 0.97 eV, and this value is smaller than the exothermic dissociation energy of H_2O (-1.06 eV or -1.57 eV to gaseous H_2O). However, it is noted that the formation of $\text{O} + \text{H}_2(\text{g})$ is exothermic by 0.42 to the adsorbed H_2O or by 0.93 eV to gaseous H_2O .

For comparison (Supporting information), we computed H_2O dissociation in the carbon region starting with the stable adsorption configuration; the transition states of H_2O dissociation into $\text{OH} + \text{H}$ and $\text{OH} + \text{H}$ dissociation into $\text{O} + 2\text{H}$ are 1.12 and 1.96 eV over gaseous H_2O , respectively. This indicates that H_2O desorbs back to the gas phase instead of dissociation in the carbon region and we

Table 1

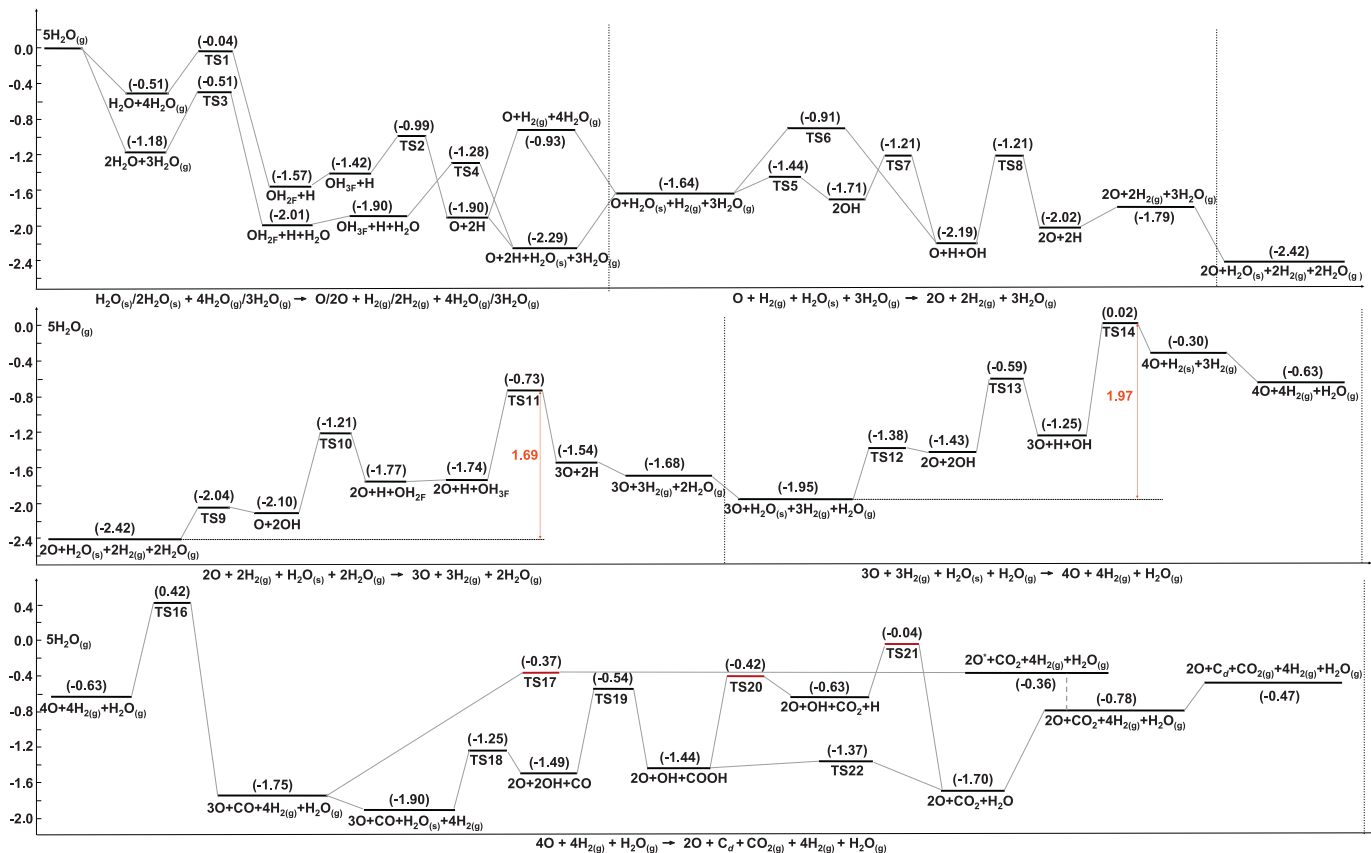
Bond distances (\AA) and adsorption energies (E_{ads} , eV) of the adsorbed H_2O , OH , O and H as well as the IS and FS for H_2O direct dissociation and H_2O dissociation at high H_2O coverage in the Fe region on the $\text{Fe}_5\text{C}_2(0\ 1\ 0)$ surface.

Configuration	E_{ads}	$E_{\text{ads}}(\text{ZPE})$	$r(\text{Fe}-\text{O})$	$r(\text{Fe}-\text{H})$
H ₂ O direct dissociation				
$\text{H}_2\text{O}_{1\text{F}}$	-0.65	-0.51	2.131	
$\text{OH}_{2\text{F}}$	-4.35	-4.24	1.956, 1.957	
$\text{O}_{3\text{F}}$	-6.65	-6.57	1.854, 1.906, 1.914	
$\text{H}_{3\text{F}}$	-3.06	-2.87		1.772, 1.773, 1.793
$\text{OH}_{2\text{F}} + \text{H}_{3\text{F}}$	-7.14	-6.81	1.965, 1.943	1.755, 1.750, 1.859
$\text{OH}_{3\text{F}} + \text{H}_{3\text{F}}$	-6.98	-6.66	1.985, 1.952, 2.135	1.761, 1.749, 1.873
$\text{O}_{3\text{F}} + 2\text{H}_{3\text{F}}$	-12.28	-11.80	1.847, 1.853, 1.942	1.761, 1.738, 1.769, 1.765, 1.713, 1.800
High coverage of H_2O				
$2\text{H}_2\text{O}_{1\text{F}}$	-1.39	-1.18	2.249, 2.146	
$\text{OH}_{2\text{F}} + \text{H}_{3\text{F}} + \text{H}_2\text{O}_{1\text{F}}$	-7.68	-7.26	2.203, 1.957, 1.955	1.710, 1.821, 1.799
$\text{OH}_{3\text{F}} + \text{H}_{3\text{F}} + \text{H}_2\text{O}_{1\text{F}}$	-7.55	-7.14	2.230, 1.970, 1.956, 2.117	1.714, 1.825, 1.801
$\text{O}_{3\text{F}} + 2\text{H}_{3\text{F}} + \text{H}_2\text{O}_{1\text{F}}$	-12.78	-12.21	2.185, 1.844, 1.850, 1.940	1.743, 1.745, 1.772, 1.753, 1.822, 1.694
$3\text{H}_2\text{O}_{1\text{F}}$	-2.11	-1.79	2.134, 2.150, 3.571	
$4\text{H}_2\text{O}_{1\text{F}}$	-2.73	-2.33	2.067, 2.133, 3.573, 3.494	

Table 2

Barriers and reaction energies (E_a and $\Delta_r E$, eV) of H_2O direct dissociation and H_2O dissociation at high coverage ($2\text{H}_2\text{O}$ co-adsorption) in the Fe region on the $\text{Fe}_5\text{C}_2(0\ 1\ 0)$ Surface, and the bond distances (r , \AA) of the transition states.

	E_a	$\Delta_r E$	$r(\text{Fe}-\text{O})$	$r(\text{Fe}-\text{H})$	$d(\text{O}-\text{H})$
$\text{H}_2\text{O} \rightarrow \text{OH} + \text{H}$ (1a); $\text{OH} + \text{H} \rightarrow \text{O} + 2\text{H}$ (2a)					
(1a) TS1	0.47	-1.06	1.963	1.823	1.333
(2a) TS2	0.43	-0.48	1.929, 1.930, 2.020	1.637, 1.770, 1.752, 1.796	1.359
$2\text{H}_2\text{O} \rightarrow \text{OH} + \text{H} + \text{H}_2\text{O}$ (1b); $\text{OH} + \text{H} + \text{H}_2\text{O} \rightarrow \text{O} + 2\text{H} + \text{H}_2\text{O}$ (2b)					
(1b) TS3	0.67	-0.83	2.219, 1.946	1.760	1.397
(2b) TS4	0.62	-0.39	2.186, 1.924, 1.915, 2.019	1.753, 1.820, 1.736, 1.635	1.376

**Fig. 4.** $\text{Fe}_x\text{C}_y + 5\text{H}_2\text{O}(\text{g}) \rightarrow \text{O}_2\text{Fe}_x\text{C}_y-1 + 4\text{H}_2(\text{g}) + \text{CO}_2(\text{g}) + \text{H}_2\text{O}(\text{g})$.

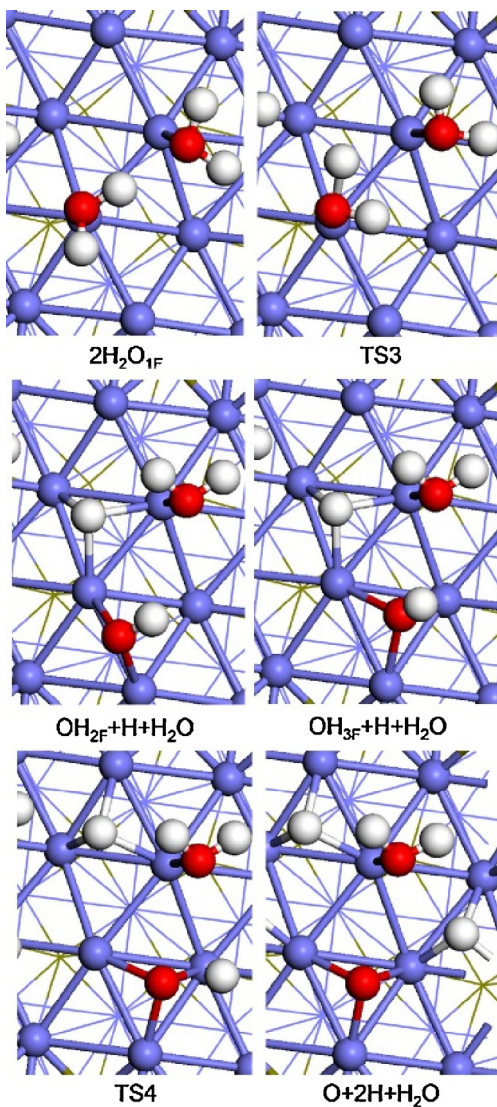


Fig. 5. Key surface structures of H_2O dissociation at high H_2O coverage in the Fe region on the $\text{Fe}_3\text{C}_2(010)$ surface (Fe atom in blue, O atom in red and H atom in white). (For interpretation of the references to color in this figure legend, the reader is referred to the web version of this article.)

therefore only paid attention to the iron region for further H_2O dissociation.

3.3. H_2O dissociation at higher coverage ($2\text{H}_2\text{O} = \text{O} + \text{H}_2(\text{g}) + \text{H}_2\text{O}$)

For the case with the increased coverage the model of two co-adsorbed H_2O molecules interacting directly with the surface iron atoms is used. The optimized structures of IS, TS and FS are shown in Fig. 5; bond parameters of IS and FS are given in Table 1; and the barriers and reaction energies as well as bond distances of TS are given in Table 2. The energy profiles are shown in Fig. 4.

For the two co-adsorbed H_2O molecules, there are two steps for H_2O dissociation: (i) $2\text{H}_2\text{O} \rightarrow \text{OH} + \text{H} + \text{H}_2\text{O}$ and (ii) $\text{OH} + \text{H} + \text{H}_2\text{O} \rightarrow \text{O} + 2\text{H} + \text{H}_2\text{O}$. The barriers are 0.67 and 0.62 eV (higher than those of one H_2O dissociation (0.47 and 0.43 eV)), and the reactions are exothermic by 0.83 and 0.39 eV (less than those in one H_2O dissociation (−1.06 and −0.48 eV)). In their transition states (TS3 and TS4), the breaking O–H distances are 1.397 and 1.376 Å, respectively. On the other hand, H_2 desorption has barrier of 0.65 eV, lower than that (0.97 eV) of one H_2O dissociation. However, it is noted that the formation of $\text{O} + \text{H}_2\text{O} + \text{H}_2(\text{g})$ is exothermic

by 1.64 eV compared to gaseous H_2O . Since one H_2O direct dissociation is more favorable both kinetically and thermodynamically than that of two co-adsorbed H_2O molecules, we paid our attention to the stepwise H_2O adsorption and dissociation on O-pre-covered surface as discussed below.

3.4. H_2O dissociation on O pre-covered surface

For the O pre-covered surface, H_2O dissociation is modeled with the stepwise increase of H_2O molecules after the formation of one H_2 , i.e.; (i) $\text{O} + \text{H}_2\text{O}(\text{g}) \rightarrow 2\text{O} + \text{H}_2(\text{g})$, (ii) $2\text{O} + \text{H}_2\text{O}(\text{g}) \rightarrow 3\text{O} + \text{H}_2(\text{g})$ and (iii) $3\text{O} + \text{H}_2\text{O}(\text{g}) \rightarrow 4\text{O} + \text{H}_2(\text{g})$. For H_2O dissociation on the O-pre-covered surfaces, the optimized structures of IS, TS and FS are shown in Figs. 6–8, respectively. The bond lengths of IS and FS are given in Table 3. The dissociation barriers, dissociation energies, and critical bond distances of TS are given in Table 4. The energy profiles are shown in Fig. 4.

Starting from one H_2O direct dissociation with the formation of $\text{O} + \text{H}_2(\text{g})$ on the clean surface, the first step of the second H_2O dissociation is modeled by the co-adsorption of the previously adsorbed surface O and one H_2O from gas phase ($\text{O} + \text{H}_2\text{O}(\text{g})$); and the computed H_2O adsorption energy for $\text{O} + \text{H}_2\text{O}$ is −0.71 eV, which is stronger than that (−0.51 eV) on the clean surface, and this difference is due to the hydrogen bonding of O and H_2O with the $\text{O}\dots\text{H}$ distance of 1.713 Å. Because of the surface O atom, H_2O can have O assisted ($\text{OH} + \text{OH}$) dissociation and one OH of $\text{OH} + \text{OH}$ further dissociates into $\text{O} + \text{H} + \text{OH}$, or direct $\text{O} + \text{H} + \text{OH}$ dissociation. Our results show that the O-assisted H_2O dissociation (0.20 eV) has a lower barrier than the direct dissociation (0.73 eV). In their transition states (TS5 and TS6), the O–H distances are elongated to 1.361 and 1.533 Å, respectively. For the dissociation of $\text{OH} + \text{OH}$ into $\text{O} + \text{H} + \text{OH}$, this step has a barrier of 0.50 eV and the O–H distance is 1.373 Å in its transition state (TS7). These indicate that the O-assisted two-step process is kinetically more favorable. For the further dissociation of $\text{O} + \text{H} + \text{OH}$ into $2\text{O} + 2\text{H}$, the computed barrier is 0.98 eV. In its transition state (TS8), the breaking O–H distance is 1.407 Å. As shown in Fig. 4, the overall reaction starting from $\text{O} + \text{H}_2\text{O}(\text{g})$ with the formation of $2\text{O} + \text{H}_2(\text{g})$ is exothermic by 0.86 eV. Compared to gaseous H_2O , this step is exothermic by 1.79 eV.

Starting from the second H_2O dissociation on the O pre-covered surface with the formation of $2\text{O} + 2\text{H}_2(\text{g})$, the first step of the third H_2O dissociation is the co-adsorption of two previously adsorbed O atoms and one H_2O from gas phase ($2\text{O} + \text{H}_2\text{O}(\text{g})$), and the computed adsorption energy for $2\text{O} + \text{H}_2\text{O}$ is −0.63 eV, which is higher than the first H_2O adsorption on the clean surface, but lower than that of the second H_2O adsorption on one O-pre-covered surface. Since O-assisted H_2O dissociation is more preferable kinetically, we considered only this reaction path and the computed barrier is 0.38 eV, and the breaking O–H distance is 1.475 Å in the transition state (TS9). The step towards the formation of $\text{O} + 2\text{OH}$ becomes endothermic by 0.32 eV, indicating that the recombination is more favorable. For the subsequent OH dissociation from $\text{O} + 2\text{OH}$ into $2\text{O} + \text{H} + \text{OH}$; and from $2\text{O} + \text{H} + \text{OH}$ into $3\text{O} + 2\text{H}$, the computed barrier is 0.89 and 1.04 eV, respectively. In their transition states (TS10 and TS11), the breaking O–H distance is 1.376 and 1.433 Å, respectively. As shown in Fig. 4, the overall reaction starting from $2\text{O} + \text{H}_2\text{O}(\text{g})$ with the formation of $3\text{O} + \text{H}_2(\text{g})$ is slightly endothermic by 0.11 eV, and the overall effective barrier is 1.69 eV. Compared to gaseous H_2O , this step is still exothermic by 1.68 eV.

Starting from the third H_2O dissociation on the 2O pre-covered surface with the formation of $3\text{O} + 3\text{H}_2(\text{g})$, the first step of the fourth H_2O dissociation is the co-adsorption of the previously adsorbed three surface O atoms and one H_2O from gas phase ($3\text{O} + \text{H}_2\text{O}(\text{g})$), and the computed H_2O adsorption energy for $3\text{O} + \text{H}_2\text{O}$ is −0.27 eV, much lower than those of the first three H_2O molecules, indicating

Table 3

Bond distances (\AA) and adsorption energies (E_{ads} , eV) of IS and FS for n O-assisted H_2O dissociation ($n = 1, 2$ and 3) in the Fe region on the $\text{Fe}_5\text{C}_2(0\ 1\ 0)$ surface.

Configuration	E_{ads}	$E_{\text{ads}}(\text{ZPE})$	$r(\text{Fe}-\text{O})$	$r(\text{Fe}-\text{H})$
O-assisted H_2O dissociation				
$\text{H}_2\text{O}_{1\text{F}} + \text{O}_{3\text{F}}$	-7.48	-7.29	2.083, 1.972, 1.887, 1.893	
$\text{OH}_{2\text{F}} + \text{OH}_{3\text{F}}$	-8.20	-7.93	2.110, 1.957, 1.997, 1.945, 1.998	
$\text{O}_{3\text{F}} + \text{H}_{3\text{F}} + \text{OH}_{2\text{F}}$	-13.49	-13.09	1.843, 1.862, 1.943, 1.940, 1.965	
$2\text{O}_{3\text{F}} + 2\text{H}_{3\text{F}}$	-18.16	-17.59	1.83, 61.834, 1.942, 1.846, 1.834, 1.950	1.753, 1.778, 1.790 1.741, 1.705, 1.785, 1.813, 1.767, 1.694
2O-assisted H_2O dissociation				
$2\text{O}_{3\text{F}} + \text{H}_{2\text{O}}_{1\text{F}}$	-14.01	-13.72	1.870, 1.966, 1.882, 1.928, 1.874, 1.918, 2.118	
$\text{O}_{3\text{F}} + 2\text{OH}_{2\text{F}}$	-14.34	-13.97	1.872, 1.878, 1.942, 1.937, 1.935, 2.139, 1.974	
$2\text{O}_{3\text{F}} + \text{H}_{3\text{F}} + \text{OH}_{2\text{F}}$	-18.85	-18.31	1.860, 1.794, 1.937, 1.904, 1.835, 1.885, 1.934, 1.982	1.671, 1.832, 1.714
$2\text{O}_{3\text{F}} + \text{H}_{3\text{F}} + \text{OH}_{3\text{F}}$	-18.80	-18.28	1.864, 1.795, 1.943, 1.901, 1.862, 1.862, 1.963, 1.958, 2.154	1.660, 1.809, 1.734
$3\text{O}_{3\text{F}} + 2\text{H}_{3\text{F}}$	-23.47	-22.76	1.856, 1.786, 1.952, 1.907, 1.813, 1.856, 1.823, 1.843, 1.887	1.687, 1.819, 1.699, 1.757, 1.646, 1.701
3O-assisted H_2O dissociation				
$3\text{O}_{3\text{F}} + \text{H}_{2\text{O}}_{1\text{F}}$	-19.29	-18.90	1.927, 1.842, 1.915, 1.871, 1.895, 1.861, 1.838, 1.837, 1.908, 2.259	
$2\text{O}_{3\text{F}} + \text{OH}_{2\text{F}} + \text{OH}_{4\text{F}}$	-19.38	-18.94	1.888, 1.861, 1.864, 1.846, 1.842, 1.907, 2.060, 1.969, 2.300, 2.133, 2.069, 2.088	
$3\text{O}_{3\text{F}} + \text{H}_{3\text{F}} + \text{OH}_{2\text{F}}$	-24.08	-23.49	1.882, 1.861, 1.847, 1.840, 1.843, 1.896, 1.940, 1.927, 2.170, 2.994, 1.896, 1.927	1.623, 1.830, 1.827
$4\text{O}_{3\text{F}} + \text{H}_{2-2\text{F}}$	-28.02	-27.44	1.871, 1.853, 1.876, 1.803, 1.868, 1.911, 1.817, 1.819, 1.901, 1.910, 1.836, 1.800	1.672, 1.684

Table 4

Barriers and reaction energies (E_a and $\Delta_r E$, eV) of n O-assisted H_2O dissociation ($n = 1, 2$ or 3) in the Fe region on the $\text{Fe}_5\text{C}_2(0\ 1\ 0)$ surface, and the bond distances (r , \AA) of the transition states.

	E_a	$\Delta_r E$	$r(\text{Fe}-\text{O})$	$r(\text{Fe}-\text{H})$	$d(\text{O}-\text{H})/\{d(\text{H}-\text{H})\}$
$\text{O} + \text{H}_2\text{O} \rightarrow 2\text{OH}$ (1c); $\text{O} + \text{H}_2\text{O} \rightarrow \text{O} + \text{H} + \text{OH}$ (2c); $2\text{OH} \rightarrow \text{O} + \text{H} + \text{OH}$ (3c); $\text{O} + \text{H} + \text{OH} \rightarrow 2\text{O} + 2\text{H}$ (4c)					
(1c) TS5	0.20	-0.07	1.943, 1.957, 2.052, 1.914		1.361
(2c) TS6	0.73	-0.55	1.913, 1.862, 1.845, 1.924	1.841	1.533
(3c) TS7	0.50	-0.48	1.931, 1.919, 2.026, 1.939, 1.969	1.635	1.373
(4c) TS8	0.98	0.17	1.839, 1.843, 1.946, 1.916, 1.866, 2.081	1.738, 1.702, 1.791, 1.629	1.407
$2\text{O} + \text{H}_2\text{O} \rightarrow \text{O} + 2\text{OH}$ (1d); $\text{O} + 2\text{OH} \rightarrow 2\text{O} + \text{H} + \text{OH}$ (2d); $2\text{O} + \text{H} + \text{OH} \rightarrow 3\text{O} + 2\text{H}$ (3d)					
(1d) TS9	0.38	0.32	1.889, 1.889, 1.879, 1.906, 1.10; 1.898		1.475, 1.376
(2d) TS10	0.89	0.33	1.866, 1.820, 1.947, 1.978, 1.866, 2.209, 1.925, 2.001	1.697	
(3d) TS11	1.04	0.23	1.860, 1.788, 1.951, 1.900, 1.840, 1.861, 1.915, 1.903, 2.095	1.688, 1.770, 1.716, 1.705	1.433
$3\text{O} + \text{H}_2\text{O} \rightarrow 2\text{O} + 2\text{OH}$ (1e); $2\text{O} + 2\text{OH} \rightarrow 3\text{O} + \text{H} + \text{OH}$ (2e); $3\text{O} + \text{H} + \text{OH} \rightarrow 4\text{O} + \text{H}_2$ (3e)					
(1e) TS12	0.57	0.52	1.867, 1.863, 1.856, 1.843, 1.839, 1.908, 2.005, 1.853, 2.001		1.341
(2e) TS13	0.84	0.18	1.879, 1.874, 1.876, 1.860, 1.845, 1.905, 1.928, 2.015; 2.247, 2.043, 2.162, 1.919	1.667	1.452
(3e) TS14	1.27	0.95	1.848, 1.850, 1.879, 1.823, 1.851, 1.902, 1.862, 1.943, 2.005, 1.914, 1.833, 1.799	1.625	1.297, {1.000}

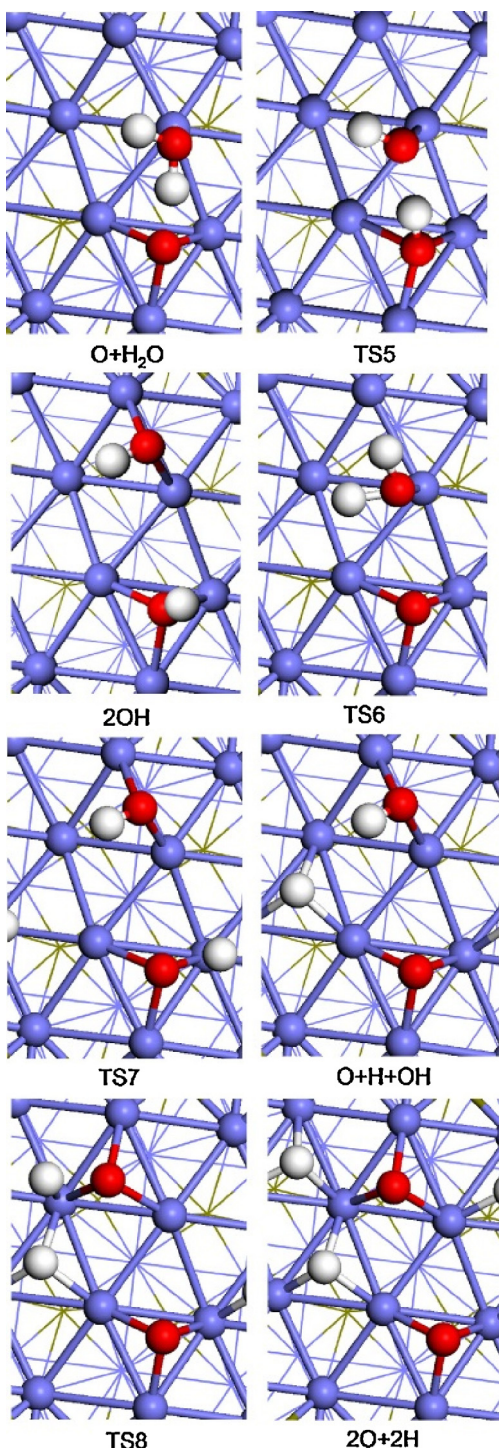


Fig. 6. Key surface structures of H_2O dissociation in the Fe region covered by one surface O atom on the $\text{Fe}_5\text{C}_2(0\ 1\ 0)$ surface (Fe atom in blue, O atom in red and H atom in white). (For interpretation of the references to color in this figure legend, the reader is referred to the web version of this article.)

the repulsive interaction between the adsorption H_2O molecule and surface O atoms. The computed O-assisted H_2O dissociation barrier into $2\text{O} + 2\text{OH}$ is 0.57 eV, and the dissociation reaction is endothermic by 0.52 eV. In its transition state (**TS12**), the breaking O-H distance is 1.341 Å. These indicate that the reverse reaction is much easier. As shown in Fig. 4, further OH dissociation steps have barriers of 0.84 eV from $2\text{O} + 2\text{OH}$ to $3\text{O} + \text{H} + \text{OH}$ and of 1.27 eV from $3\text{O} + \text{H} + \text{OH}$ to $4\text{O} + \text{H}_2(\text{s})$; and the breaking O-H distance in their

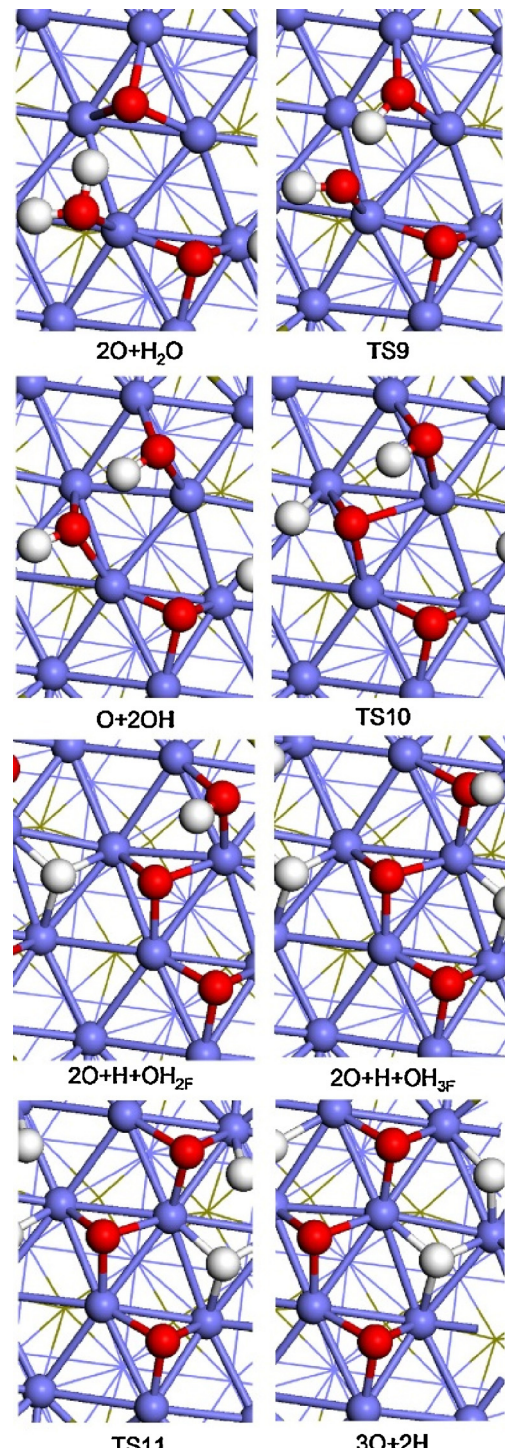


Fig. 7. Key surface structures of H_2O dissociation in the Fe region covered by two surface O atoms on the $\text{Fe}_5\text{C}_2(0\ 1\ 0)$ surface (Fe atom in blue, O atom in red and H atom in white). (For interpretation of the references to color in this figure legend, the reader is referred to the web version of this article.)

transition states (**TS13** and **TS14**) is 1.452 and 1.297 Å, respectively. All these steps are endothermic, and the overall effective barrier is as high as 1.97 eV. It is noted that the formation of $\text{H}_2(\text{g})$ from the co-adsorbed $4\text{O} + \text{H}_2(\text{s})$ is exothermic by 0.33 eV, indicating that with the increased O coverage, H_2 formation becomes easier, while H_2O dissociation becomes more difficult. The highest point (**TS14**) on the potential energy surface (0.02 eV) is as high as gaseous H_2O ,

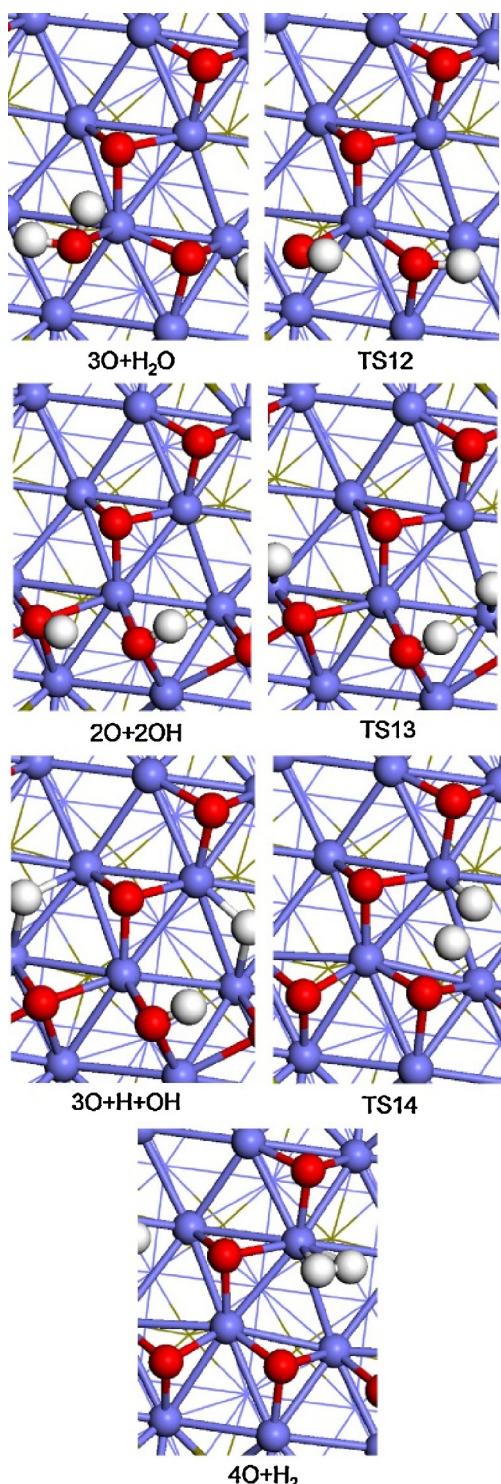


Fig. 8. Key surface structures of H_2O dissociation in the Fe region covered by three surface O atoms on the $\text{Fe}_5\text{C}_2(0\bar{1}0)$ surface (Fe atom in blue, O atom in red and H atom in white). (For interpretation of the references to color in this figure legend, the reader is referred to the web version of this article.)

and the overall reaction is still exothermic by 0.63 eV. With four O atoms in the iron region, the iron region is fully covered.

3.5. Thermodynamics

Since Thüne et al. [4i] found that water can affect the stability of iron oxide and iron carbide nanoparticles strongly and surface

iron(II) oxide plays an important role by regulating the relative rate of CO hydrogenation versus WGS reaction and by stabilizing the iron carbide catalyst against irreversible deactivation by oxidation to magnetite, we have calculated the structure and stability of atomic oxygen covered Fe_5C_2 surface by using thermodynamic approach under the consideration of the gas environment. Table S6 lists the change of the Gibbs energies along with the change of the number of the deposited oxygen atoms in the temperature range of 500–700 K at defined $\text{H}_2\text{O}/\text{H}_2$ partial pressure ratios (Supporting information). Fig. S4 shows the surface structures with two to six adsorbed oxygen atoms (Supporting information).

At very low $\text{H}_2\text{O}/\text{H}_2$ ratio (10^{-4}), the stable surface has only two adsorbed oxygen atoms within 500–700 K. At $\text{H}_2\text{O}/\text{H}_2 = 10^{-3}$, the surface can have three adsorbed oxygen atoms, but only stable at temperature below 500 K. At $\text{H}_2\text{O}/\text{H}_2 = 0.01$, the surface with three adsorbed oxygen atoms becomes possible, but only stable at temperature below 650 K. Further increase of the $\text{H}_2\text{O}/\text{H}_2$ ratios from 0.1 to 2, the stable surface has three adsorbed oxygen atoms within 500–700 K. At high $\text{H}_2\text{O}/\text{H}_2$ ratios from 2.5 to 10, the surface with four adsorbed oxygen atoms becomes stable at different temperatures, e.g.; at temperature below 500 K for $\text{H}_2\text{O}/\text{H}_2 = 2.5$, at temperature below 550 K for $\text{H}_2\text{O}/\text{H}_2 = 5$ and at temperature below 600 K for $\text{H}_2\text{O}/\text{H}_2 = 10$. Within these constraints, it is not possible to have more than four adsorbed oxygen atoms on the surface. On the basis of our result and the fact that water is a principal FTS product, it is reasonably to conclude that the iron-based active catalysts in FTS should always have some adsorbed oxygen atoms on the surface and these oxygen atoms are in balance in formation and removal. That lowering temperature and increasing $\text{H}_2\text{O}/\text{H}_2$ ratios can increase the oxidation degree of the surface is in agreement with the findings by Thüne et al. [4i].

3.6. Surface carbon oxidation

Since the carbon region is not competitive in H_2O adsorption and dissociation with the iron region, we are interested in surface carbon oxidation by the adsorbed oxygen atoms from the iron region. Since the number of the adsorbed oxygen atoms in the iron region depends on water content, we used the surfaces with three and four adsorbed oxygen atoms as our models, respectively. For the surface with three adsorbed oxygen atoms, the energy profiles and the corresponding structures are shown in Fig. 9. For four oxygen atoms covered surface, the optimized structures of IS, TS and FS are shown in Fig. 10. The bond lengths of IS and FS are given in Table 5.

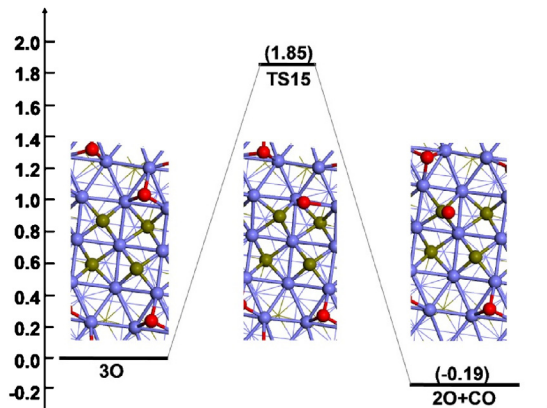


Fig. 9. Structures of IS, TS and FS and barrier for the surface carbon oxidation to CO by three surface O atoms formed in H_2O dissociation (Fe atom in blue, O atom in red and H atom in white). (For interpretation of the references to color in this figure legend, the reader is referred to the web version of this article.)

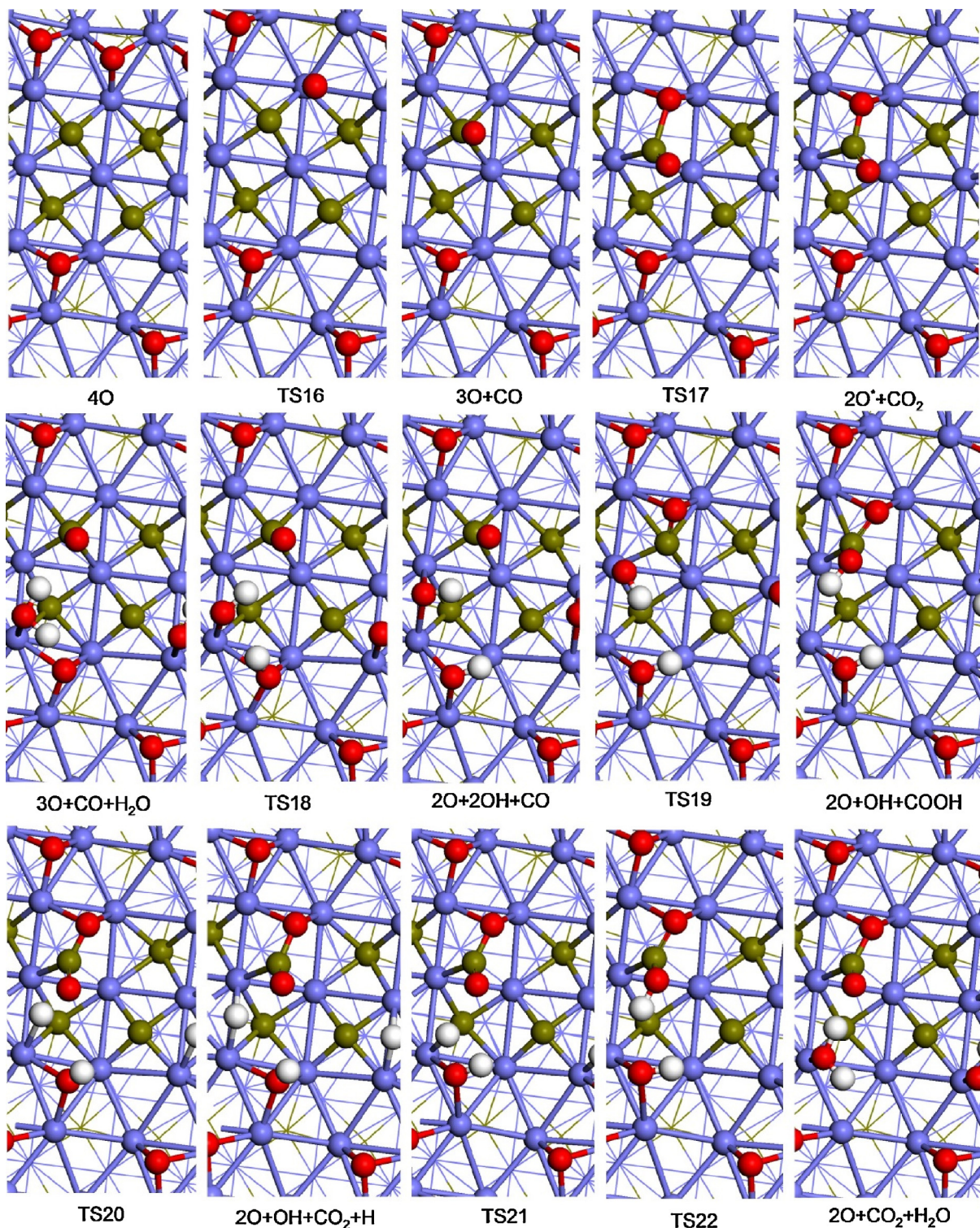


Fig. 10. Key surface structures of surface carbon oxidation into CO_2 from surface O in the iron region for direct oxidation and H_2O assisted reaction via carboxylic (COOH) intermediate (Fe atom in blue, O atom in red, C atom in dark orange and H atom in white). (For interpretation of the references to color in this figure legend, the reader is referred to the web version of this article.)

The barriers, reaction energies, and critical bond distances of the TS are listed in Table 6. The energy profiles are also shown in Fig. 4.

Starting from 3O pre-adsorbed surface, one O atom diffusion to the carbon region forming surface CO ($2\text{O} + \text{CO}$) has barrier of 1.85 eV, and the reaction is exothermic by 0.19 eV. In the transition state (TS15), the O atom is at bridge site and the forming C-O distance is 1.766 Å. Starting from 4O pre-adsorbed surface, one O atom diffusion to the carbon region forming surface CO ($3\text{O} + \text{CO}$)

has barrier of 1.05 eV, and the reaction is exothermic by 1.12 eV. In the transition state (TS16), the O atom is at top site and the forming C-O distance is 1.887 Å. This shows that surface carbon atoms can only be oxidized by surface with four adsorbed oxygen atoms.

For the subsequent oxidation of the formed CO in the carbon region into CO_2 , we have calculated both the direct and H_2O mediated oxidations. For the direct oxidation, one oxygen atom in the iron region attaches the adsorbed CO in the carbon region

Table 5

Bond distances (\AA) and adsorption energies (E_{ads} , ev) of IS and FS of surface carbon oxidation into CO_2 from surface O in the iron region for direct oxidation and H_2O associated reaction via carboxylic (COOH) intermediate on the $\text{Fe}_5\text{C}_2(0\ 1\ 0)$ surface.

Configuration	E_{ads}	$E_{\text{ads}}(\text{ZPE})$	$r(\text{Fe}-\text{O})$	$r(\text{Fe}-\text{C})/\{r(\text{Fe}-\text{H})\}$	$r(\text{C}-\text{O})$
Oxidation of C_s with 30					
$3\text{O}_{3\text{F}}$	-18.90	-18.63	1.860, 1.820, 1.918, 1.887, 1.843, 1.876, 1.830, 1.839, 1.906		
$2\text{O}_{3\text{F}} + \text{CO}_{4\text{F}}$	-19.04	-18.81	1.861, 1.847, 1.929, 1.860, 1.868, 1.912	2.003, 2.128, 2.208, 2.039	
Oxidation of C_s with 40					
$4\text{O}_{3\text{F}}$	-23.62	-23.22	1.840, 1.850, 1.914, 1.860, 1.846, 1.884, 1.812, 1.826, 1.882, 1.800, 1.837, 1.905		
$3\text{O}_{3\text{F}} + \text{CO}_{4\text{F}}$	-24.68	-24.35	1.842, 1.822, 1.925, 1.839, 1.888, 1.876, 1.865, 1.823, 1.900	2.004, 2.149, 2.218, 2.036	1.213
$2\text{O}_{3\text{F}} + \text{CO}_{2-3\text{F}}$	-23.28	-22.96	1.816, 1.852, 1.925, 1.811, 1.884, 1.915, 1.901, 2.162	2.007	1.406, 1.257
$3\text{O}_{3\text{F}} + \text{CO}_{4\text{F}} + \text{H}_2\text{O}_{1\text{F}}$	-24.91	-24.49	1.815, 1.906, 1.948, 1.857, 1.895, 1.877, 1.832, 1.905, 1.869, 2.256	2.011, 2.135, 2.150, 2.016	1.234
$2\text{O}_{3\text{F}} + 2\text{OH}_{2\text{F}} + \text{CO}_{4\text{F}}$	-25.19	-24.66	1.843, 1.925, 1.850, 1.869, 1.829, 1.898, 2.011, 1.934, 2.011, 1.962	2.084, 2.154, 2.088, 1.996	1.223
$2\text{O}_{3\text{F}} + \text{OH}_{2\text{F}} + \text{COOH}_{4\text{F}}$	-25.20	-24.59	1.842, 1.922, 1.849, 1.843, 1.854, 1.887, 2.018, 1.976, 2.046, 2.170	1.891, 2.296	1.310, 1.349
$2\text{O}_{3\text{F}} + \text{OH}_{2\text{F}} + \text{CO}_{2-3\text{F}} + \text{H}_{2\text{F}}$	-29.15	-28.47	1.877, 1.937, 1.857, 1.846, 1.862, 1.890, 1.973, 1.991, 2.015, 1.975, 2.033	{1.639, 1.677}, 1.983	1.377, 1.239
$2\text{O}_{3\text{F}} + \text{CO}_{2-3\text{F}} + \text{H}_2\text{O}_{1\text{F}}$	-24.75	-24.30	1.916, 1.868, 1.879, 1.847, 1.863, 1.898, 1.987, 2.106, 2.045	1.948	1.354, 1.247
$2\text{O}_{3\text{F}} + \text{CO}_{2-3\text{F}}$	-23.71	-23.37	1.918, 1.865, 1.882, 1.845, 1.855, 1.895, 2.013, 2.061	1.952	1.377, 1.257
$2\text{O}_{3\text{F}} + \text{C}_d$	-13.09	-12.93	1.940, 1.861, 1.879, 1.887, 1.838, 1.925		

Table 6

Barriers and reaction Energies (E_a and $\Delta_r E$, eV) of surface carbon oxidation into CO_2 from surface O in the iron region for direct oxidation and H_2O associated reaction via carboxylic (COOH) intermediate on the $\text{Fe}_5\text{C}_2(0\ 1\ 0)$ surface, and the bond distances (r , \AA) of the transition states.

	E_a	$\Delta_r E$	$r(\text{Fe}-\text{O})$	$r(\text{Fe}-\text{C})/\{r(\text{Fe}-\text{H})\}$	$r(\text{C}-\text{O})$	$d(\text{O}-\text{H})/\{d(\text{C}-\text{O})\}$
$3\text{O} + \text{C}_s \rightarrow 2\text{O} + \text{C}_s\text{O}$ (1f)						
(1f) TS15	1.85	-0.19	1.873, 1.828, 1.922, 1.945, 1.883, 1.881, 1.921, 2.147			{1.766}
$4\text{O} + \text{C}_s \rightarrow 3\text{O} + \text{C}_s\text{O}$ (1g)						
(1g) TS16	1.05	-1.12	1.830, 1.839, 1.914, 1.850, 1.887, 1.861; 1.879, 1.861, 1.888, 1.837			{1.887}
$3\text{O} + \text{CO} \rightarrow 2\text{O}^* + \text{CO}_2$ (2g)						
(2g) TS17	1.38	1.39	1.819, 1.854, 1.919, 1.814, 1.823, 1.916, 1.834, 1.917	1.915	1.187	{1.717}
$3\text{O} + \text{CO} + \text{H}_2\text{O} \rightarrow 2\text{O} + 2\text{OH} + \text{CO}$ (3g)						
(3g) TS18	0.65	0.41	1.869, 1.886, 1.873, 1.869, 1.834, 1.902, 1.907, 2.023, 2.212, 1.933	2.049, 2.149, 2.116, 1.994	1.229	1.770
$2\text{O} + 2\text{OH} + \text{CO} \rightarrow 2\text{O} + \text{OH} + \text{COOH}$ (4g)						
(4g) TS19	0.95	0.05	1.845, 1.920, 1.853, 1.844, 1.849, 1.891, 1.998, 2.003, 2.091, 2.255	1.953, 1.871, 2.275, 2.247	1.263	{2.010}
$2\text{O} + \text{OH} + \text{COOH} \rightarrow 2\text{O} + \text{OH} + \text{H} + \text{CO}_2$ (5g)						
(5g) TS20	1.02	0.81	1.867, 1.912, 1.860, 1.849, 1.857, 1.892, 1.961, 1.983, 2.134, 2.038, 2.218	1.912, [1.816]	1.316, 1.282	1.491
$2\text{O} + \text{OH} + \text{H} + \text{CO}_2 \rightarrow 2\text{O} + \text{H}_2\text{O} + \text{CO}_2$ (6g)						
(6g) TS21	0.59	-1.07	1.848, 1.931, 1.851, 1.847, 1.859, 1.894, 2.027, 2.267, 1.988, 2.089	1.949, [1.607]	[1.357, 1.236]	1.371
$2\text{O} + \text{OH} + \text{COOH} \rightarrow 2\text{O} + \text{H}_2\text{O} + \text{CO}_2$ (7g)						
(7g) TS22	0.07	-0.26	1.849, 1.921, 1.860; 1.846, 1.858, 1.891, 1.913, 2.352, 2.015, 2.283	1.892	1.307, 1.337	

($3\text{O} + \text{CO} \rightarrow 2\text{O} + \text{CO}_2$), and the calculated barrier is 1.38 eV and the reaction is endothermic by 1.39 eV, indicating the trend of CO_2 dissociation rather than CO_2 formation, and therefore such direct oxidation is very unlikely. In the transition state (**TS17**), the forming C–O distance is 1.717 Å.

As an alternative way of the direct oxidation, H_2O mediated oxidation has been conducted. At first, one H_2O molecule adsorbs atop at the vacant site between the iron and carbon regions. With the formation of the adsorption configuration of $3\text{O} + \text{CO} + \text{H}_2\text{O}$, the computed adsorption energy is exothermic by 0.15 eV. Dissociation of the adsorbed H_2O results in the formation of two surface hydroxyls ($2\text{O} + 2\text{OH} + \text{CO}$), one in the iron region and one in the carbon region, the computed barrier is 0.65 eV, and the dissociation is endothermic by 0.41 eV. In the transition state (**TS18**), the breaking O–H distance is 1.770 Å. Since the formed hydroxyl in the carbon region is close to the previously formed surface CO, they can interact and form surface carboxyl ($2\text{O} + \text{OH} + \text{COOH}$). The formation of $2\text{O} + \text{OH} + \text{COOH}$ has barrier of 0.95 eV and is slightly endothermic by 0.05 eV. In the transition state (**TS19**), the OH group is at the top site and the forming C–O distance is 2.010 Å.

The formed COOH can either dissociate directly into $2\text{O} + \text{OH} + \text{CO}_2 + \text{H}$ or interacts with its neighboring OH to give $2\text{O} + \text{H}_2\text{O} + \text{CO}_2$. For the direct dissociation ($2\text{O} + \text{OH} + \text{COOH} \rightarrow 2\text{O} + \text{OH} + \text{CO}_2 + \text{H}$), the calculated barrier is 1.02 eV and the reaction is endothermic by 0.81 eV. The breaking O–H distance in **TS20** is 1.491 Å. In addition, in the configuration of $2\text{O} + \text{OH} + \text{CO}_2 + \text{H}$, the H atom can combine the surface OH back to H_2O ($2\text{O} + \text{OH} + \text{CO}_2 + \text{H} \rightarrow 2\text{O} + \text{H}_2\text{O} + \text{CO}_2$), and the calculated barrier is 0.59 eV, and the reaction is exothermic by 1.07 eV. In the transition state (**TS21**), and the forming O–H distance is 1.371 Å. Starting from $2\text{O} + \text{OH} + \text{COOH}$ to $2\text{O} + \text{H}_2\text{O} + \text{CO}_2$ via the direct pathway, the effective barrier is 1.40 eV.

For the OH mediated COOH dissociation ($2\text{O} + \text{OH} + \text{COOH} \rightarrow 2\text{O} + \text{H}_2\text{O} + \text{CO}_2$), the first step is the migration of the OH group from the bridge site to the top site via transition state (**TS22**), and the calculated barrier is very low (0.07 eV), and the subsequent CO_2 and H_2O formation does not require barriers and the formation of $2\text{O} + \text{CO}_2 + \text{H}_2\text{O}$ is exothermic by 0.26 eV. Compared with the high effective barrier (1.40 eV) of the direct pathway, the OH mediated pathway is much more favorable kinetically.

The potential energy surface in Fig. 4 shows clearly that H_2O mediated surface carbon oxidation is more favorable than the direct oxidation, and the most favored reaction path has the intermediate of $2\text{O} + \text{OH} + \text{COOH}$, which dissociates into $2\text{O} + \text{H}_2\text{O} + \text{CO}_2$ without barriers. The overall surface carbon oxidation is $\text{Fe}_x\text{C}_y + 4\text{H}_2\text{O}(\text{g}) \rightarrow \text{O}_2\text{Fe}_{x-y} + \text{CO}_2(\text{g}) + 4\text{H}_2(\text{g})$. Our results show that surface carbon oxidation is only possible at very high H_2O partial pressure and low temperature. With the desorption of the formed CO_2 from the surface, four additional iron atoms are exposed on the surface, which can initiate further H_2O dissociation and surface carbon oxidation and finally results in full oxidation. Our results reveal clearly that the catalysts should have adsorbed oxygen atoms on the surfaces, and the stability of the catalysts can be maintained by either reducing H_2O content or increasing the temperature, and excess H_2O content results in full oxidation. Our results are in full agreement with the recent findings Thüne et al. [41] in studying the effect of water on the stability of iron oxide and iron carbide nanoparticles in hydrogen and synthesis gas.

3.7. Comparison of H_2O dissociation on iron surfaces and iron region of $\text{Fe}_5\text{C}_2(0\ 1\ 0)$

Now it is interesting to compare the oxidation properties of the iron region on $\text{Fe}_5\text{C}_2(0\ 1\ 0)$ and metallic iron surface by H_2O . Metallic iron has been considered as one of the active phase in iron-based FTS. There are several studies about H_2O adsorption and

Table 7
 H_2O dissociation barriers (eV) on $\text{Fe}(1\ 0\ 0)$ and $\text{Fe}_5\text{C}_2(0\ 1\ 0)$.

	$\text{Fe}(1\ 0\ 0)$	$\text{Fe}_5\text{C}_2(0\ 1\ 0)$
$\text{H}_2\text{O} \rightarrow \text{OH} + \text{H}$	1.0 ^a ; 0.68 ^b ; 0.35 ^c ; 0.16 ^d	0.47 ^e
$\text{OH} \rightarrow \text{O} + \text{H}$	0.8 ^a ; 0.91 ^b ; 0.79 ^c ; 0.62 ^d	0.58 ^e
$(\text{H}_2\text{O})_2 \rightarrow \text{H}_2\text{O}(\text{OH}) + \text{H}$	1.25 ^a	0.67 ^e
$\text{H}_2\text{O} + \text{O} \rightarrow \text{OH} + \text{OH}$	0.03 ^d	0.20 ^e

^a Ref [18g].

^b Ref [18f].

^c Ref [18d].

^d Ref [18e].

^e Current work.

dissociation on iron surfaces both experimentally [17] and theoretically [18]. Table 7 lists the computed H_2O dissociation barriers on $\text{Fe}(1\ 0\ 0)$ and $\text{Fe}_5\text{C}_2(0\ 1\ 0)$ for comparison.

On the $\text{Fe}(1\ 0\ 0)$ surface [17a–d], H_2O adsorbs molecularly at low temperature and low coverage, while dissociatively at high temperature. H_2O dissociation forms not only surface hydroxyl (OH) but also atomic oxygen and molecular H_2 . Further oxidation of $\text{Fe}(1\ 0\ 0)$ by H_2O adsorption results in a saturated oxygen coverage of 0.39 mL. Similar results were found on the $\text{Fe}(0\ 0\ 1)$ [17e] and $(1\ 1\ 0)$ [17f] surfaces. Such adsorption and dissociation phenomena have been found by computations [18]. On the iron region of the $\text{Fe}_5\text{C}_2(0\ 1\ 0)$ surface, H_2O dissociations also lead to a higher coverage of surface oxygen and H_2 desorption. Using DFT calculations Jung et al. [18d] showed that the H_2O molecular state is subject to dissociation into $\text{H} + \text{OH}$ species with a barrier of 0.35 eV, OH dissociation into $\text{H} + \text{O}$ species requires a higher energy of 0.79 eV. Goverder et al. [18e] and Lazar et al. [18f] also studied the two steps of the dissociation of H_2O to $\text{OH} + \text{H}$ then into $\text{O} + 2\text{H}$, and found that the activation energies are 0.16 and 0.62 eV, as well as 0.68 and 0.91 eV, respectively. DFT calculations by Freitas et al. [18g] showed that on the $\text{Fe}(1\ 0\ 0)$ surface the dissociation barrier for $\text{H}_2\text{O} \rightarrow \text{OH} + \text{H}$ and $\text{OH} \rightarrow \text{O} + \text{H}$ is 1.0 and 0.8 eV, respectively, and at the coverage of two adsorbed H_2O molecules, the dissociation barrier for $\text{H}_2\text{O} \rightarrow \text{OH} + \text{H}$ increases to 1.25 eV. This is the same as found in the iron region on the $\text{Fe}_5\text{C}_2(0\ 1\ 0)$ surface, i.e.; the dissociation barrier for the single H_2O process is 0.47 and 0.58 eV, respectively, and that for the two H_2O process increases to 0.67 eV. This shows that H_2O dissociation on $\text{Fe}_5\text{C}_2(0\ 1\ 0)$ is slightly easier than on $\text{Fe}(1\ 0\ 0)$.

On one O-pre-covered $\text{Fe}(1\ 0\ 0)$ surface, Govender et al. [18e] found that the dissociation barrier for $\text{H}_2\text{O} + \text{O}$ to form $\text{OH} + \text{OH}$ is reduced to 0.03 eV. On one O-pre-covered $\text{Fe}_5\text{C}_2(0\ 1\ 0)$ surface, the barrier for $\text{H}_2\text{O} + \text{O}$ to form $\text{OH} + \text{OH}$ is reduced to 0.20 eV, and the barrier for $\text{H}_2\text{O} + \text{O}$ to form $(\text{OH} + \text{H}) + \text{O}$ is 0.73 eV as well as the barrier for $(\text{OH} + \text{H}) + \text{O}$ to $(\text{O} + \text{H}) + \text{O} + \text{H}$ is 0.98 eV. This shows the similarity between one O-pre-covered $\text{Fe}(1\ 0\ 0)$ and $\text{Fe}_5\text{C}_2(0\ 1\ 0)$ surfaces. However, results for H_2O dissociation on more than one O-pre-covered $\text{Fe}(1\ 0\ 0)$ surfaces are not available.

4. Conclusion

H_2O adsorption and dissociation on the $\text{Fe}_5\text{C}_2(0\ 1\ 0)$ surface have been investigated using spin-polarized density functional theory computations (GGA–PBE). The $\text{Fe}_5\text{C}_2(0\ 1\ 0)$ surface has both iron and carbon regions, and on the basis of the computed adsorption energies, the iron region is active for H_2O adsorption and dissociation, while the carbon region is inactive.

With the increased H_2O coverage in the iron region, not only H_2O adsorption but also hydrogen bonding interaction among the co-adsorbed H_2O molecules become important as found on the basis of the computed adsorption configurations and energies as well as

the non-bonded intermolecular O–H distances; and the computed hydrogen bonding energies are in the range of the reported values.

At low coverage direct H₂O dissociation (H₂O → H + OH; OH → H + O) in the iron region is highly favored kinetically and thermodynamically; and the highest barrier is only 0.47 eV and its total reaction energy is exothermic by 0.93 eV. Despite of the fact that H₂O dissociation into surface O and gaseous H₂ is thermodynamically favorable on the potential surface, atomic H adsorption instead of molecular H₂ formation is more favored by 0.97 eV. It is also found that high H₂O coverage (co-adsorption of two H₂O molecules) does not affect the potential energy significantly apart from the hydrogen bonding interaction.

On one O pre-covered surface, O-assisted H₂O dissociation becomes favorable kinetically (O + H₂O → OH + OH) and last OH dissociation (OH → H + O) becomes difficult kinetically and thermodynamically. In addition, atomic H adsorption instead of molecular H₂ formation is more favored by 0.23 eV, which is less than that on the clean surface.

With the increase of surface O coverage, H₂O dissociation becomes more difficult kinetically and thermodynamically. For 2O pre-covered surface, H₂O dissociation is endothermic by 0.74 eV, and the effective barrier is 1.69 eV; and molecular H₂ formation becomes more favored than atomic H adsorption by 0.14 eV. For 3O pre-covered surface H₂O dissociation is endothermic by 1.32 eV, and the effective barrier is 1.97 eV; and molecular H₂ formation becomes more favored than atomic H adsorption by 0.33 eV. These energetic changes are just the opposite to those on the clean and one O pre-covered surfaces, and these show the strong coverage effect in H₂O dissociation ability on the partially oxidized surfaces. On the potential energy surface, although the stepwise H₂O dissociation becomes more difficult upon the increased partial oxidation of the surface, the dissociation of four H₂O molecules into four surface O and four H₂ molecules (4H₂O(g) → 4O(s) + 4H₂(g)) is still thermodynamically favored by 0.63 eV. High similarities in H₂O adsorption and dissociation on iron region on Fe₅C₂(0 1 0) and on Fe(1 0 0) have been found.

Thermodynamic analysis shows that the stable Fe₅C₂(0 1 0) surface under water environment is always covered by oxygen atoms, and their number depends on water content and temperature. From very low to very high H₂O content, the adsorbed surface oxygen atoms change from three to four at different temperature. At very high H₂O content, the surface carbon can also be oxidized by the adsorbed oxygen atoms from the iron region, and this will lead to full oxidation of the catalysts. Therefore, it is possible to maintain the catalyst stability by adjusting H₂O content, i.e.; by lowering H₂O content and increasing temperature. Our results are fully supported by the recent experimental studies.

For the oxidation of surface carbon atom to CO₂, the first step is the migration of one of the four adsorbed surface oxygen atoms to form surface CO. On the potential energy surface, the H₂O-assisted pathway with the formation of surface intermediates from H₂O dissociation (2O + 2OH + CO), and COOH formation from CO and OH coupling is more favorable than the direct pathway. The overall surface carbon oxidation, Fe_xC_y + 4H₂O(g) → O₂Fe_xC_y-1 + CO₂(g) + 4H₂(g), is thermodynamically favorable by 0.47 eV.

Acknowledgments

This work was supported by the National Natural Science Foundation of China (no. 21273262 & 21273266), the National Basic Research Program of China (no. 2011CB201406), the Chinese Academy of Science and Synfuels CHINA. Co., Ltd.

Appendix A. Supplementary data

Supplementary data associated with this article can be found, in the online version, at <http://dx.doi.org/10.1016/j.apcata.2013.09.017>.

References

- [1] (a) M.E. Dry, *Hydrocarb. Process.* 61 (1982) 121–124;
 (b) J.J.C. Geerlings, J.H. Wilson, G.J. Kramer, H.P.C.E. Kuipers, A. Hoek, H.M. Huisman, *Appl. Catal., A* 186 (1999) 27–40;
 (c) M.E. Dry, *Catal. Today* 71 (2002) 227–241;
 (d) J.M. Fox III, *Catal. Rev. Sci. Eng.* 35 (1993) 169–212;
 (e) J.H. Gregor, *Catal. Lett.* 7 (1990) 317–331;
 (f) J. Cheng, P. Hu, P. Ellis, S. French, *Top. Catal.* 53 (2010) 326–337.
- [2] (a) A.K. Datye, Y.M. Jin, L. Mansker, R.T. Motjope, T.H. Dlamini, N.J. Coville, *Stud. Surf. Sci. Catal.* 130B (2000) 1139–1144;
 (b) Y.M. Jin, L. Mansker, A.K. Datye, *ASC, Div. Pet. Chem.* 44 (1999) 97–99;
 (c) Y.Q. Zhang, R.J. O'Brien, B.H. Davis, H.H. Hamdeh, *ASC, Div. Pet. Chem.* 44 (1999) 100–102;
 (d) B.H. Davis, *Catal. Today* 84 (2003) 83–98;
 (e) W. Ning, N. Koizumi, H. Chang, T. Mochizuki, T. Itoh, M. Yamada, *Appl. Catal., A* 312 (2006) 35–44;
 (f) P.G. Caceres, *Mater. Charact.* 56 (2006) 26–31.
- [3] (a) D.B. Cao, F.Q. Zhang, Y.W. Li, H. Jiao, *J. Phys. Chem. B* 108 (2004) 9094–9104;
 (b) D.B. Cao, F.Q. Zhang, Y.W. Li, H. Jiao, *J. Phys. Chem. B* 109 (2005) 833–844;
 (c) D.B. Cao, F.Q. Zhang, Y.W. Li, H. Jiao, *J. Phys. Chem. B* 109 (2005) 10922–10935;
 (d) D.B. Cao, S.G. Wang, Y.W. Li, H. Jiao, *J. Mol. Catal. A: Chem.* 272 (2007) 275–287;
 (e) P.J. Steynberg, J.A. van den Berg, W.J. van Rensburg, *J. Phys. Condens. Matter* 20 (064238) (2008) 11;
 (f) D.C. Sorescu, *J. Phys. Chem. C* 113 (2009) 9256–9274;
 (g) M.A. Petersen, J.A. van den Berg, W.J. van Rensburg, *J. Phys. Chem. C* 114 (2010) 7863–7879.
- [4] (a) D.B. Bokur, M. Koranne, X. Lang, K.R.M. Rao, G.P. Huffman, *Appl. Catal., A* 126 (1995) 85–113;
 (b) H. Hayakawa, H. Tanaka, K. Fujimoto, *Appl. Catal., A* 310 (2006) 24–30;
 (c) S.Z. Li, R.J. O'Brien, G.D. Meitzner, H. Hamdeh, B.H. Davis, E. Iglesia, *Appl. Catal., A* 219 (2001) 215–222;
 (d) D.J. Duvenhage, R.L. Espinoza, N.J. Coville, *Catal. Deactivat.* 88 (1994) 351–358;
 (e) D.J. Duvenhage, N.J. Coville, *Appl. Catal., A* 298 (2006) 211–216;
 (f) R.J. Gormley, M.F. Zarochak, P.W. Deffenbaugh, K.R.P.M. Rao, *Appl. Catal., A* 161 (1997) 263–279;
 (g) M.E. Dry, T. Shingles, L.J. Boshoff, *J. Catal.* 25 (1972) 99–104;
 (h) J.Z. Shultz, W.K. Hall, B. Seligman, R.B. Anderson, *J. Am. Chem. Soc.* 77 (1955) 213–221;
 (i) P. Thüne, P. Moodley, F. Scheijen, H. Fredriksson, R. Lancee, J. Kropf, J. Miller, J.W. Niemantsverdriet (Hans), *J. Phys. Chem. C* 116 (2012) 7367–7373;
 (j) V.R.R. Pendyala, G. Jacobs, J.C. Mohandas, M. Luo, H.H. Hussein, Y. Ji, M.C. Ribeiro, B.H. Davis, *Catal. Lett.* 140 (2010) 98–105;
 (k) F.G. Botes, *Catal. Rev.* 50 (2008) 471–491.
- [5] D.B. Cao, Y.W. Li, J. Wang, H. Jiao, *J. Mol. Catal. A: Chem.* 346 (2011) 55–69.
- [6] (a) G. Kresse, J. Furthmüller, *Comput. Mater. Sci.* 6 (1996) 15–50;
 (b) G. Kresse, J. Furthmüller, *Phys. Rev. B: Condens. Matter* 54 (1996) 11169–11186.
- [7] (a) P.E. Blochl, *Phys. Rev. B: Condens. Matter* 50 (1994) 17953–17979;
 (b) G. Kresse, *Phys. Rev. B: Condens. Matter* 59 (1999) 1758–1775.
- [8] J.P. Perdew, K. Burke, M. Ernzerhof, *Phys. Rev. Lett.* 77 (1996) 3865–3868.
- [9] H. Jónsson, G. Mills, K.W. Jacobsen, *Classical and Quantum Dynamics in Condensed Phase Simulations*, World Scientific, Singapore, 1998, pp. 385–404.
- [10] K.H. Jack, S. Wild, *Acta Crystallogr. S*21 (1966) A81.
- [11] A. Königer, C. Hammerl, M. Zeitler, B. Rauschenbach, *Phys. Rev. B: Condens. Matter* 55 (1997) 8143–8147.
- [12] C.F. Huo, Y.W. Li, J.G. Wang, H. Jiao, *J. Am. Chem. Soc.* 131 (2009) 14713–14721.
- [13] (a) F. Zasada, W. Piskorz, S. Cristol, J.F. Paul, A. Kotarba, Z. Sojka, *J. Phys. Chem. C* 114 (2010) 22245–22253;
 (b) Y. Aray, A.B. Vidal, J. Rodriguez, M.E. Grillo, D. Vega, D.S. Coll, *J. Phys. Chem. C* 113 (2009) 19545–19557;
 (c) P. Geysermans, F. Finocchi, J. Goniakowski, R. Hacquart, J. Jupille, *Phys. Chem. Chem. Phys.* 11 (2009) 2228–2233.
- [14] (a) S. Meng, E.G. Wang, S. Gao, *Phys. Rev. B: Condens. Matter* 69 (195404) (2004) 13;
 (b) A.A. Phatak, W.N. Delgass, F.H. Ribeiro, W.F. Schneider, *J. Phys. Chem. C* 113 (2009) 7269–7276;
 (c) J. Ren, S. Meng, *J. Am. Chem. Soc.* 128 (2006) 9282–9283;
 (d) A. Michaelides, A. Alavi, D.A. King, *J. Am. Chem. Soc.* 125 (2003) 2746–2755;
 (e) G.C. Wang, S.X. Tao, X.H. Bu, *J. Catal.* 244 (2006) 10–16.
- [15] A. Hodgson, S. Haq, *Surf. Sci. Rep.* 64 (2009) 381–451.
- [16] (a) V.A. Ranea, A. Michaelides, R. Ramirez, P.L. de Andres, J.A. Verges, D.A. King, *Phys. Rev. Lett.* 92 (136104) (2004) 4;

- (b) Q.L. Tang, Z.X. Chen, *Surf. Sci.* 601 (2007) 954–964;
(c) A. Michaelides, *Faraday Discuss.* 136 (2007) 287–297.
- [17] (a) W.H. Hung, J. Schwartz, S.L. Bernasek, *Surf. Sci.* 248 (1991) 332–342;
(b) W.H. Hung, J. Schwartz, S.L. Bernasek, *Surf. Sci.* 294 (1993) 21–32;
(c) S.L. Bernasek, *Annu. Rev. Phys. Chem.* 44 (1993) 265–298;
(d) A.M. Baró, W. Erley, *J. Vac. Sci. Technol.* 20 (1982) 580–583;
(e) D.J. Dwyer, G.W. Simmons, R.P. Wei, *Surf. Sci.* 64 (1977) 617–632;
(f) D.J. Dwyer, S.R. Kelemen, A. Kaldor, *J. Chem. Phys.* 76 (1982) 1832–1838.
- [18] (a) A.B. Anderson, *Surf. Sci.* 105 (1981) 159–176;
- (b) M. Eder, K. Terakura, J. Hafner, *Phys. Rev. B: Condens. Matter* 64 (115426) (2001) 7;
(c) P. Błoński, A. Kiejna, J. Hafner, *J. Phys. Condens. Matter* 19 (096011) (2007) 8;
(d) S.C. Jung, M.H. Kang, *Phys. Rev. B: Condens. Matter* 81 (115460) (2010) 7;
(e) A. Goverder, D.C. Ferré, J.W. Niemantsverdriet, *ChemPhysChem* 13 (2012) 1583–1590;
(f) P. Lazar, M. Otyepka, *J. Phys. Chem. C* 116 (2012) 25470–25477;
(g) R.R.Q. Freitas, R. Rivelino, F. de Brito Mora, C.M.C. de Castilho, *J. Phys. Chem. C* 116 (2012) 20306–20314.